Foam evolution in a processed liquid solution

2017 J. Phys.: Conf. Ser. 796 012042

(http://iopscience.iop.org/1742-6596/796/1/012042)

Foam evolution in a processed liquid solution

E Salerno[1], P Levoni[1,2], G S Barozzi[1] and A Malfatto[3]

[1] DIEF- Dipartimento di Ingegneria "Enzo Ferrari", Università di Modena e Reggio Emilia, Via Vivarelli 10 - 41125 Modena (Italy)
[2] MIMESIS fluid dynamics & energy, Strada Contrada 309 - 41126 Modena (Italy)
[3] Sidel S.p.A., Via La Spezia 241/A - 43125 Parma (Italy)

Email: elisabetta.salerno@unimore.it

Abstract. Foam formation in a carbonated solution undergoing pouring and decompression is investigated with the use of high-speed imaging. Operational conditions similar to those encountered in industrial bottling processes are applied to inspect the mechanisms that control the foaming behaviour in practical filling applications. The evolution of the foam column during pressure release is analysed in quantitative terms by extracting the foam thickness from the images. The bubble dynamics inside the solution, and the destabilization processes on the foam column are seen to have a paramount effect on the observed foam evolution trend. The contributions to foam formation given by the nuclei entrained in the bulk liquid and by the bubble-generating sites on the container walls are finally distinguished and discussed.

1. Introduction

Foams frequently arise in industrial applications involving filling and pouring of liquids, such as food processing, casting of molten metals, and pharmaceuticals and chemicals manufacturing. In those processes, the formation of foam is an unwanted effect, since it retards the production process and can compromise the product quality. Consequently, finding suitable strategies able to inhibit the inception of foam is of primary importance in those fields.

It is now well known that in practical situations the presence of pre-formed gaseous nuclei is an essential factor for a solution to foam [1]. These nuclei can be as small to escape optical detection [2], and may be introduced in the liquid by several mechanisms, including bubble entrainment by liquid-liquid impacts [3–6], and bubble entrapment along the container walls during filling [7, 8]. The growth of nuclei to macroscopic sizes may be activated by pressure reduction or temperature increase, which can drive the system to a supersaturation state [1]. The turbulent dynamics generated inside the container can also trigger the growing of nuclei by cavitation [9]. Once they reach a critical size, bubbles migrate towards the free surface of the liquid where their aggregation gives rise to a column of foam. On the other hand, foam will decay spontaneously over time, its deterioration being dictated by the kinetics of four processes: disproportionation, gas diffusion, drainage and coalescence [10–12].

The mechanisms governing foam growth and stability, as well as their influencing parameters, have been extensively studied in different research areas for many years. However, most of the published studies consider one single phenomenon at a time, and are usually performed under simplified conditions. For these reasons, the exact incidence of the various processes on the production of foam is still quite unclear; this is especially true in the context of the filling processes, where a variety of mechanical and fluid dynamical events are interrelated. The present research aims at clarifying for the first time the contributions given by the totality of the foaming mechanisms to foam formation in a

carbonated liquid, as a consequence of the pressure-filling process and the subsequent decompression phase. For this purpose, a series of experiments was carried out on a carbonated, optically transparent commercial soft drink, poured into a bottle with the use of a testing filling machine. High-speed imaging was adopted to inspect the phenomena occurring inside and above the solution, which was processed under realistic conditions of pressure and flow rate. The comparison between the images obtained on the foam column and inside the solution allowed the identification of the main phenomena at the basis of foam development. The recorded image sequences were also analysed in quantitative terms and the trend of the foam level during decompression was reconstructed.

2. Experimental procedures

2.1. Experimental set-up

In order to reproduce the fluid dynamical conditions encountered in practical filling applications, a testing filling machine for the bottling of carbonated beverages was employed in the experimentation. The machine transfers the liquid product from a pressurised reservoir to the container at controlled conditions of pressure and flow rate – their values being those typically used in the beverage industry. The container used for the tests was a brand-new 1.5 l plastic bottle. Since a swirl-type valve was used for filling, the bottle was chosen of cylindrical body, having an almost constant diameter (d = 88 mm), not ribbed and with a smoothly curved shoulder, to prevent accidental detachments of the annular filling jet from the container walls. The working fluid was carbonated on site to 4.3 volumes of CO_2, and maintained at the fixed temperature of 17.5 °C.

Experiments were performed with the following filling procedure: first, the internal pressure of the bottle was equated to the reservoir pressure, set at 4.4 bar gauge. This was achieved by introducing carbon dioxide in the bottle while venting to the atmosphere the air contained. Next, the liquid was injected into the bottle at a specific constant flow rate. The bottle was filled only partially, i.e. to just 1 l, to prevent foam overflows and allow an accurate measurement of the foam level. After the filling was completed, a short settling period was waited and then the pressure was gradually released. The decompression was operated in two steps, by consecutively opening a snift valve connected to ambient air. The opening time for second snift (Δt_2) was three times the opening time of the first snift (Δt_1), and equalled the intermediate rest period (Δt_{rest}) set between the two decompressions. The actual duration of each step cannot be provided since protected by non-disclosure agreement. At the end of each filling sequence, the bottle was emptied out, rinsed and dripped.

High-speed imaging was used for the recording of foam and bubble dynamics during decompression. The imaging system was arranged as sketched in figure 1.a. Two NanoSense MkIII CMOS cameras from Dantec Dynamics were positioned on one side of the filling machine for the simultaneous observation of the flow phenomena in distinct regions of the bottle. Two different configurations were implemented. In the first configuration (configuration A), one camera was zoomed in the bottle headspace to capture foam evolution, while the other one monitored the rising bubbles close to liquid/foam interface. The cameras were fitted with a zoom lens (AF Nikkor 28-80 mm) and a macro lens (Micro Nikkor 60 mm f/2.8), respectively. In the second configuration (configuration B), both the cameras were focused inside the liquid at different heights. In this case, they were equipped with macro lens to inspect bubble dynamics in the whole filled volume at the maximum achievable spatial resolution. Magnifications up to 100 µm/pixel were obtained. Image distortions in the liquid due to the bottle cylindrical geometry were minimized by encasing the bottle into a square-sided Plexiglas container. The optical compensation box, shown in figure 1.b, was filled with water for the matching of the refractive indexes.

Image sequences were recorded at 200 fps, which was the maximum rate compatible with the duration of the experiments. Acquisitions started at the beginning of the decompression sequence, triggered by a signal transmitted by the filling machine to the cameras. The microcontroller Arduino Uno was employed for the signal handling. A maximum synchronization error of 6.6 µs was measured, including the contribution of the cables. Three 27.2 W/m LED tubes were used as the light

sources in backlight configuration. The tubes were positioned close to the test container to provide intense illumination. A uniform distribution of light was obtained by interposing a light diffuser between the LED sources and the compensation box.

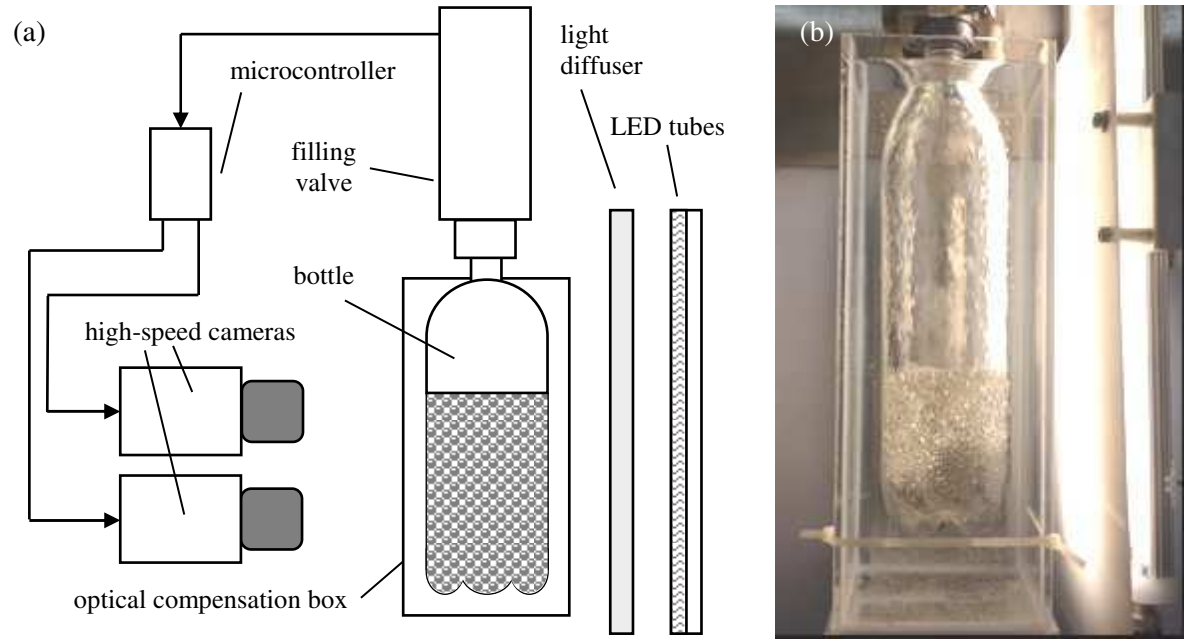

Figure 1. Schematic of the imaging system in side view (a), and snapshot of the bottle encased in the optical compensation box during filling (b).

2.2. Data reduction

The extrapolation of qualitative and quantitative information on the foam evolution and bubble behaviour was performed by processing the acquired images with the software ImageJ (provided by NIH, USA). Images collected inside the liquid were examined by direct visual inspection. No automated detection techniques could be applied because of the very high bubble concentration. The size of the bubbles was evaluated by approximating the nuclei with ellipsoids, from whose volume the equivalent spherical diameter was calculated. Subpixel accuracy could be obtained with this method.

For the estimate of the foam thickness, a procedure based on the extraction of intensity profiles was implemented. Images acquired in the bottle headspace were first filtered to suppress noise, and then reduced to a region with an almost uniform background. The profiles of the pixel intensities were drawn for the frames of interest, by plotting the horizontally averaged grey value along the vertical direction of the selected area. Each curve was analysed to identify the position of the upper and lower foam interface according to pre-determined mathematical criteria. The thickness of the foam was thus derived, with a maximum error of 9%.

3. Results and discussion

To allow the comparison between acquisitions recorded in different configurations, a preliminary repeatability analysis was carried out. The test was repeated twenty times with the cameras set in configuration A. The observed foam behaviour was qualitatively the same in all the cases; moreover, the maximum foam thickness was obtained at the same time instant with an error of 3%, its measured values showing a variation of 5%. Hence, the process can be considered reproducible.

The experiment was then performed again in both configurations. The foaming phenomena visualized inside and above the liquid during decompression are detailed in the following section.

Next, the trend of the foam level as reconstructed from a whole recorded sequence is presented and commented.

3.1. Foam and bubble dynamics

The inspected foam and bubble dynamics were divided into five main stages, here described in chronological order in terms of the dimensionless parameter $t' = t / \Delta t_1$. Exemplifying image sequences are provided, reporting i) in the first column, foam evolution as captured by the camera focused in the bottle headspace in configuration A, and ii) in the second and third column, what observed for the same time instant in the upper and lower portions of the liquid, respectively, with the cameras set in configuration B. The beginning of the first decompression step is taken as the reference time.

3.1.1. Early growth. At the beginning of the decompression stage, foam has not developed yet. As shown in figure 2.a, just a collar of bubbles is occasionally present, formed by the nuclei introduced by the impinging filling jet and already risen to the liquid free surface. Further clustering is prevented by the tail-end of the jet which is still descending along the bottle walls. The liquid bulk is populated by a large amount of bubbles having different size and distribution (figures 2.b and 2.c). They all originate from entrainment processes taking place during filling. Bubble diameters ranging from 260 μm, which is the minimum perceivable size, to 4.83 mm have been measured. The biggest bubbles are found in the upper portion of the fluid, in rapid ascension driven by buoyancy. Below this region, bubble mean diameter gradually decreases downwards. Sub-millimetric nuclei prevail in the bottom of the bottle: such small bubbles are more affected by the liquid flow field, and are easily carried down deep into the fluid where they are retained even for long times.

Within the first four tenths of the first decompression step, all the entrained bubbles having diameters larger than 2 mm before decompression reach the free surface. Their aggregation gives rise to the first layer of foam, displayed in figure 2.d. Meanwhile, the gaseous nuclei gradually increase in size due to pressure reduction. Inside the liquid, this results in some alterations of the motion of the bubbles: as the buoyancy force increases, the nuclei which are already pointing upwards are accelerated towards the free surface, while those entangled in the fluid flow become able to overcome drag. This second effect is obtained when a critical diameter is attained, which depends on the residual agitation level of the liquid. At this stage of the process, the critical diameter is on the order of the millimetre: a sudden change in direction has been observed for bubbles with diameter of 1.27 ± 0.12 mm in the upper portion of the fluid (figure 2.e) and of 1.11 ± 0.08 mm in the lower portion (figure 2.f). The slight difference between the two regions is symptomatic of a fluid velocity field which is still non-uniform.

Bubble enlargement produces, as an additional consequence, the appearance of free nuclei that before were too small to be detected. Furthermore, at nearly $t' = 0.4$ also gaseous cavities entrapped on the bottle internal walls become visible. Hence, the liquid seems pervaded by an increasingly greater amount of bubbles, as can be observed by scrolling down the images in the second and third column of figure 2. Such a trend continues in the next few instants ($0.4 < t' < 0.8$). In this time-interval no more bubbles come into view, but a few nucleation sites on the walls activate and start to release bubbles of some hundreds of microns in diameter, with frequencies as high as 24 bubbles per second.

The population of nuclei in the liquid undergoes changes also in size distribution. Since bigger bubbles rise more rapidly, the lower portion of the bottle soon remains occupied by nuclei of homogeneously small size, whose diameter grows in time up to nearly 0.6 mm. The upper portion of the bottle houses a more varied population, bubbles arriving at the liquid-foam interface with diameters of even 2.3 mm. Fed by the continuous arrivals of bubbles, the foam column keeps growing (figure 2.g). During expansion, deterioration processes begin to affect the top layers of the foam: bubble burst occurs when an unstable size is reached, as a consequence of the pressure decrease or due to coalescence between adjacent nuclei.

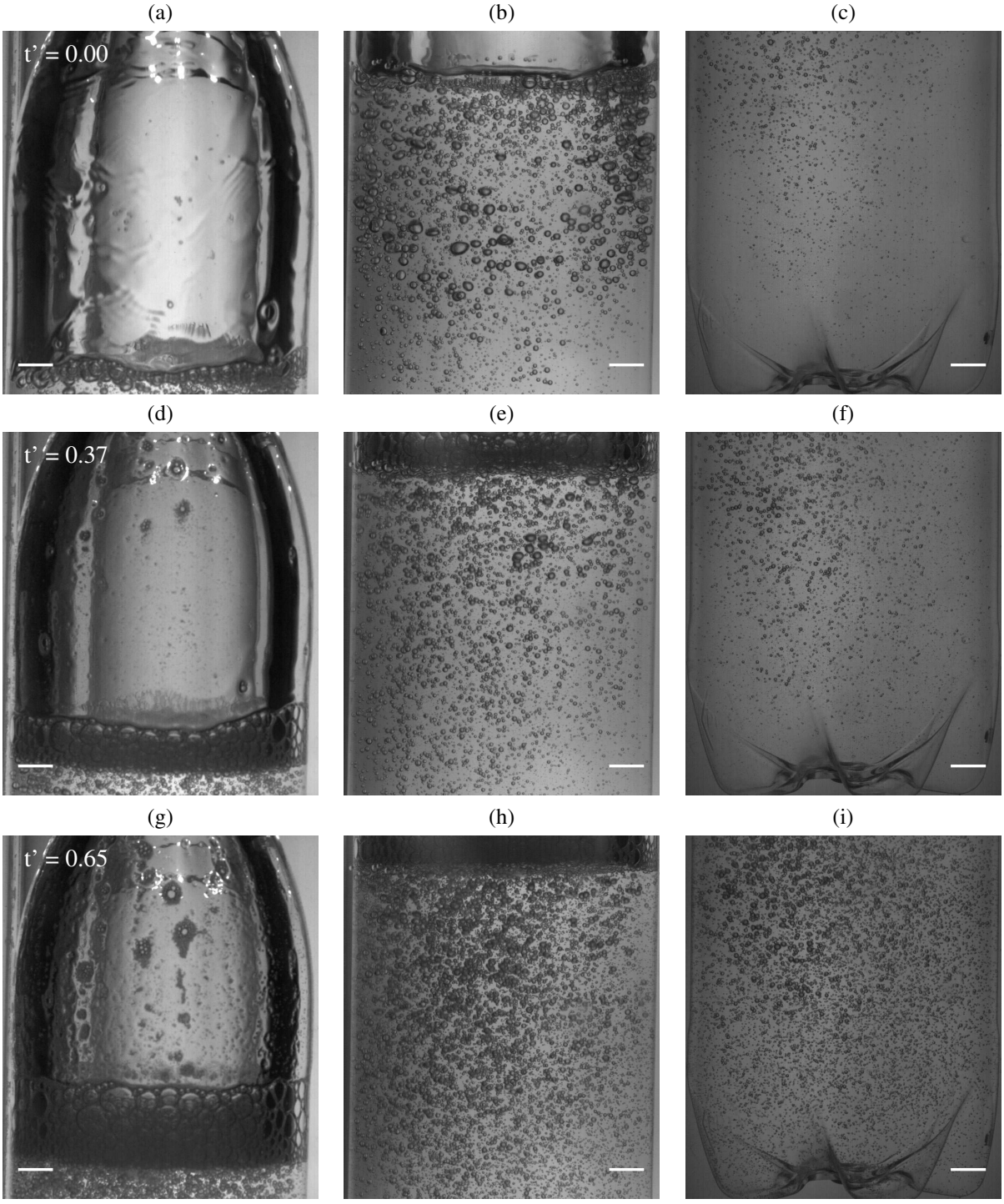

Figure 2. *Early growth.* Scale bar 10 mm.

3.1.2. Cloud formation. At about t' = 0.8, bubbles moving in the liquid bulk experience a global upward deviation of their trajectories. Visually, such a behaviour translates into the formation of a cloud of bubbles departing from the bottom of the bottle (figures 3.b and 3.c). The phenomenon is dictated by the smallest entrained nuclei left in the liquid that change direction simultaneously once they get the critical size. Relative to the previous stage, the current measured value of the critical

diameter is lower, i.e. of 0.69 ± 0.11 mm, and identical in the whole fluid, suggesting that the flow field has attenuated and levelled out. Besides the nuclei responsible of its generation, the also cloud incorporates i) entrained bubbles, typically of bigger size, already moving towards the free surface, ii) bubbles previously released from the sites on the walls, iii) entrained bubbles of size even smaller than the critical one, dragged into the wake of the rising bubbles, and, iv) bubbles torn away from the solid surface by the cloud passage.

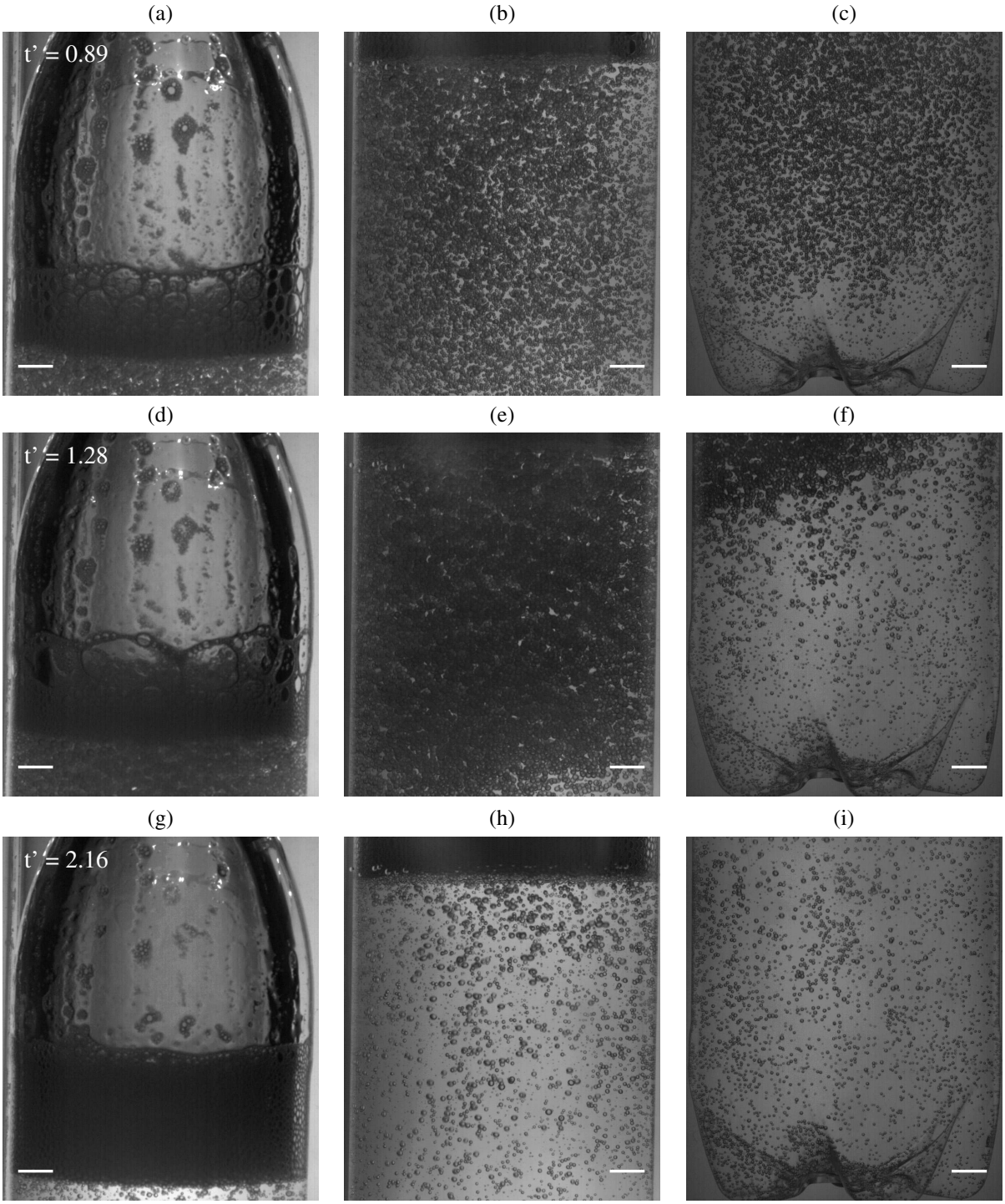

Figure 3. *Cloud formation.* Scale bar 10 mm.

While ascending, the nuclei continue to enlarge and the cloud thickens. Since the path of the nuclei is more and more obstructed, their speed is slowed down and it takes about 1.4 Δt_1 for the cloud to rise completely. Hence, the process completes at t' = 2.2 (third row of figure 3), that is, well after the end of the first decompression step, extending over the first third of the intermediate rest period. Images shown in the first column of figure 3 demonstrate that cloud ascent promotes a significant expansion of the foam column. However, foam growth is not constant. On the one hand, it is interrupted by coalescence and burst of the bubbles composing the upper (and older) layers of the foam, like the ones appearing in figure 3.d. On the contrary, the new layers formed by the bubbles carried by the cloud are more compact and homogeneous, and so more stable. On the other hand, the interface between the liquid and foam is not fixed: initially the developing gaseous phase inside the liquid makes the interface shift upwards. As the cloud evolves, the rising nuclei start to crowd at progressively lower levels, and the interface is brought back to nearly the starting height.

3.1.3. First collapse. With the cloud passage, the liquid empties out of all the nuclei introduced by entrainment. Nucleation sites already identified on the bottle walls continue to release bubbles in the remaining part of the intermediate rest period ($2.2 < t' < 4.0$), but with progressively slower rates. Further sites between the ones visible in figures 3.h and 3.i become active in this stage. These, in general, produce a few bubbles, whose size and frequency of release are highly influenced by interactions with other nuclei. Due to the scarce supply of new bubbles, the foam behaviour is dominated by decay. The homogeneous structure of the foam hinders its immediate deterioration. With passing time, drainage and coalescence induce structural changes in the whole foam column, involving fusion, deformation and rearrangement of bubbles, as can be observed by comparing figures 3.g and 4.a. As a result, bubble skins get thinner and weaker, ultimately causing the rupture of the top layers of the foam.

3.1.4. Second growth and collapse. The second decompression step, operated at t' = 4.0, is instantly perceived as a sudden but moderate swelling of the bubbles in the foam. The foam structure is then further destabilized and subsequently exposed to a faster decay. Indeed, figures 5.a and 5.d show that the foam height drops, ultimately assuming, at t' = 5.3, levels similar to those observed in the very early stages of the process (figure 2.d). The new pressure decrease also affects the bubbles inside the liquid, including those bound to the bottle walls. As can be seen from the images in figures 5.b and 5.c, as compared with figures 4.b and 4.c, the bubble diameter increases rapidly, up to 30% in the first three tenths of the second snift.

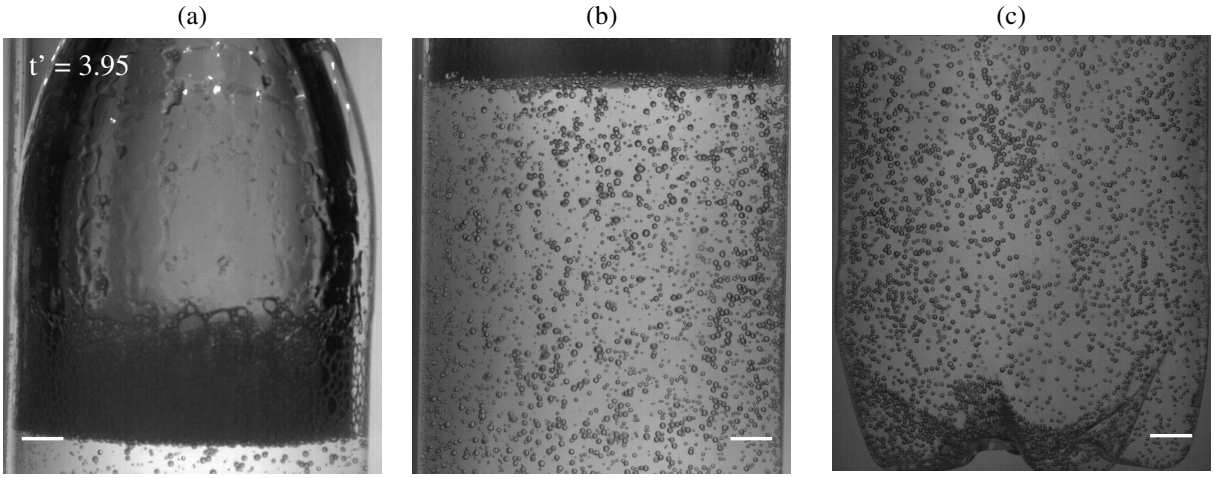

Figure 4. *First collapse.* Scale bar 10 mm.

The persistence of a supersaturation state in the liquid promotes the growth of the nuclei also in the following instants. Consequently, more bubbles become able to overcome adhesion and detach from the solid surface. Large bubbles from the bottom of the bottle stimulate, in turn, the release of other nuclei when bumping them during ascension. In addition, nucleation sites activated during the first snift recover their original frequencies of release. All those factors produce a gradual increment in the rate of bubbles arriving at the liquid-foam interface (figure 5.b). Such a tendency culminates at approximately t' = 4.8, after which no apparent variations in the characteristics of the emerging bubbles are observed.

3.1.5. Final equilibrium. When t' > 5.5 the foam height stops reducing. Any decay of the existing layers is compensated by the massive arrival of new bubbles, as large as those responsible of the generation of the first layer of foam. Hence the foam column is progressively deprived of residual bubbles from the first decompression step, which are substituted by freshly originated nuclei of uniform size. This process contributes to create an equilibrium state which lasts till the end of the process, as proved by figure 6. From figure 6.c it is also evident that despite the augmenting buoyancy force and the collisions with rising nuclei, clusters of bubbles are held on the bottle walls. These may give an additional delayed contribution to the foam, as they can be activated by mechanical agitation once the bottle is detached from the filling machine.

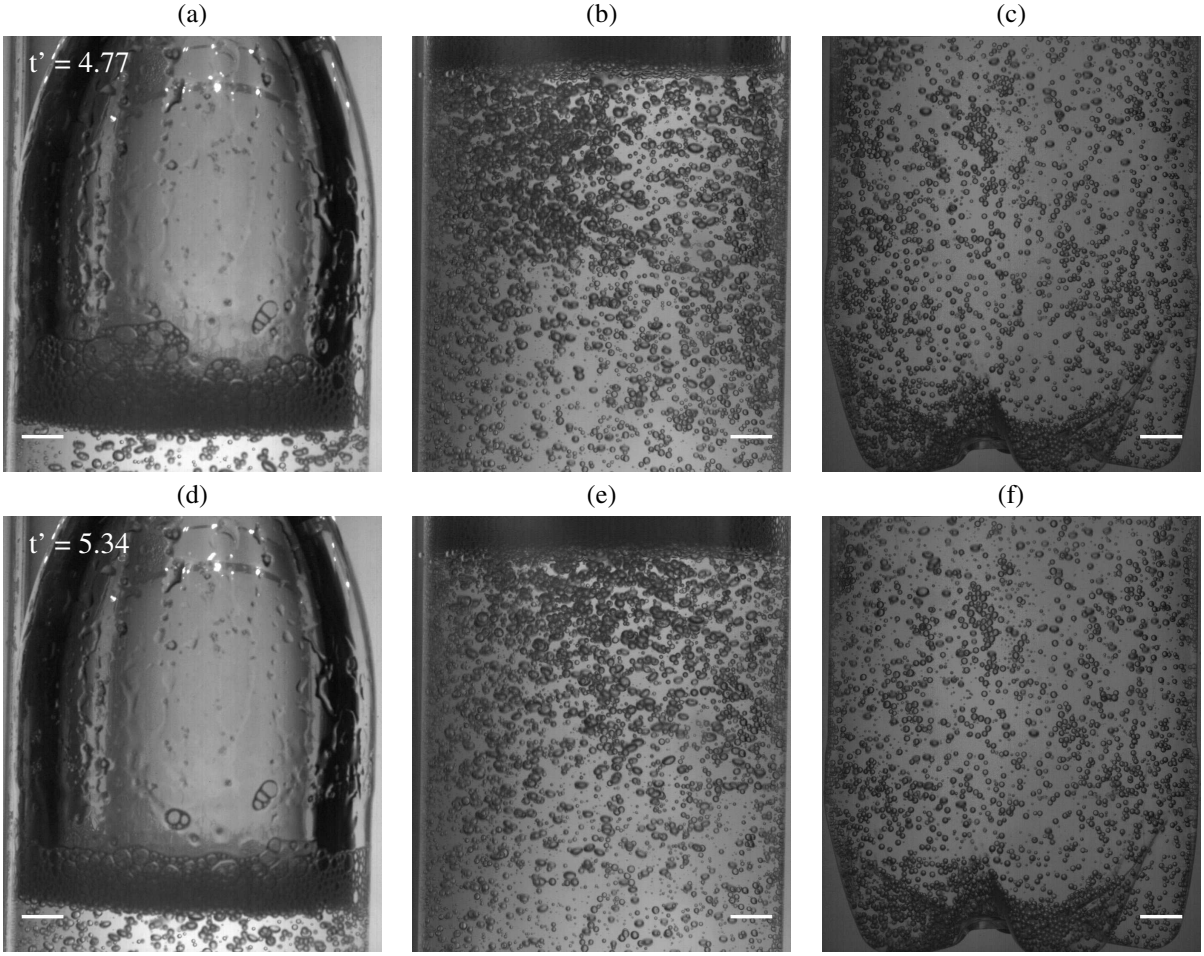

Figure 5. *Second growth and collapse.* Scale bar 10 mm.

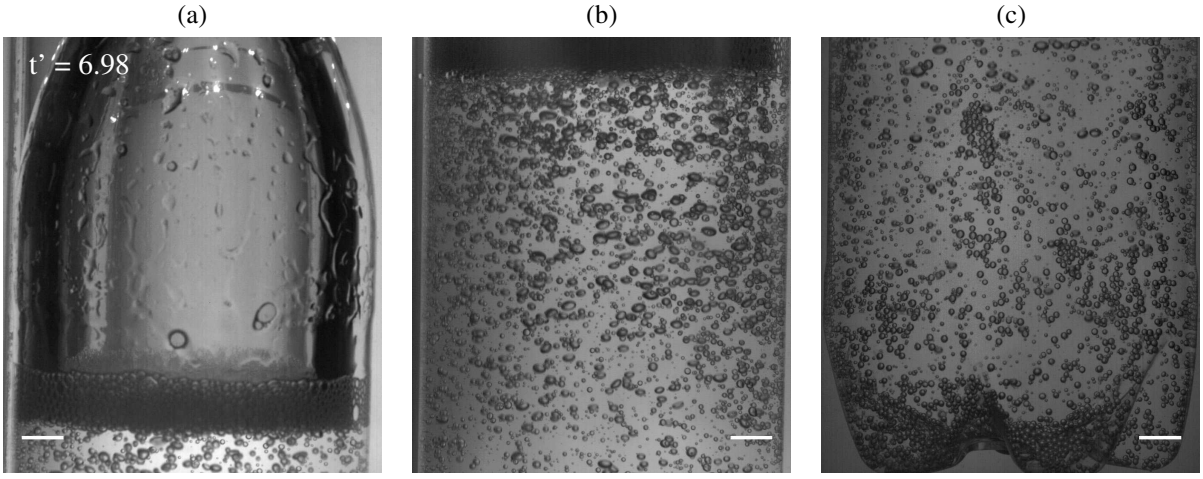

Figure 6. *Final equilibrium.* Scale bar 10 mm.

3.2. Plot of the foam trend

To understand how the above foaming dynamics reflect on the amount of foam produced, the image sequence relative to configuration A was analysed in quantitative terms. The foam thickness was extracted from 86 frames using the procedure described in section 2.2. The measurements were intensified when rapid changes in the foam column were observed, so as to reconstruct the whole trend with the best accuracy. The resulting graph of the foam thickness versus time is displayed in figure 7. Boundaries between the different stages of the decompression sequence are also indicated.

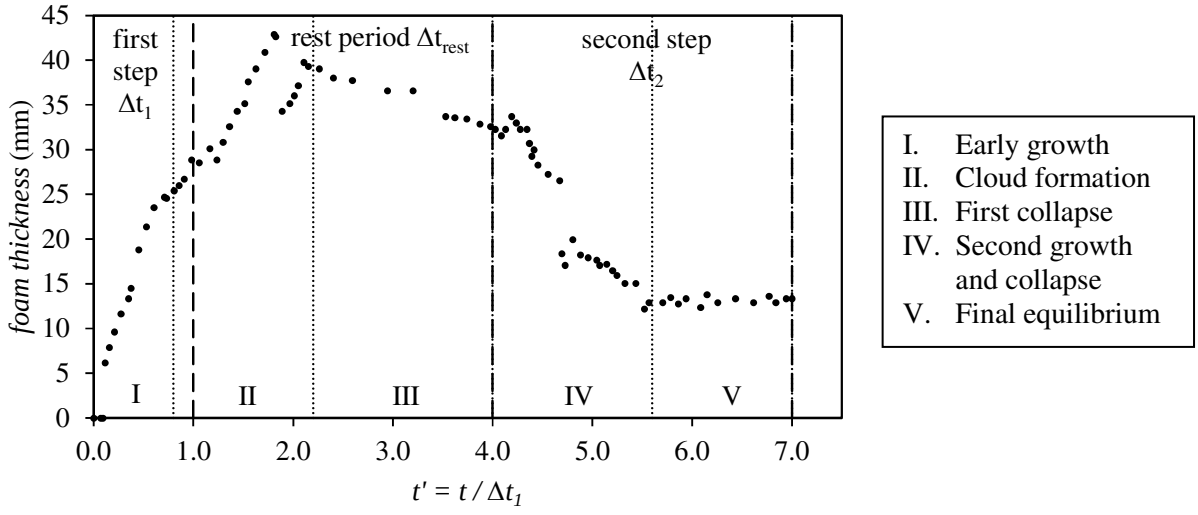

Figure 7. Graph of the foam level versus time. Dashed and dotted lines represent the boundaries between i) the decompression steps and ii) the identified stages of foaming dynamics, respectively.

The graph shows that the foam level grows rapidly during the first half of the first decompression step, fostered by the rise of the largest entrained bubbles. The growth is not immediate, but a short latency time has to be waited to allow the aggregation of the initial layer of foam. Later, the foam continues to expand with a slower rate. The change in slope should be attributed to variations occurring in the population of the ascending nuclei, such as their mean diameter and rising velocity. Nevertheless, the subsequent generation and development of the cloud, as reported in section 3.1.2,

produce a further increase in the foam thickness. Bumps are present in this segment of the curve; these are caused by the occasional burst of bubbles on the top of the column. Though the cloud has not completely risen, at t' = 1.8 the foam reaches its maximum thickness, i.e. 43 mm, corresponding to the 26 % of the filled volume of liquid. The subsequent rupture of a large bubble originated by fusion from those visible in figure 3.d produces a sudden drop in the foam height. Next, the level is partially restored by the tail nuclei of the cloud as they eventually reach the liquid-foam interface.

With the cloud arrival (t' = 2.2), the production of foam induced by the first decompression step ceases. On the contrary, the foam level starts to decrease despite the incoming of some residual bubbles from the bottle walls. Initially (2.2 < t' < 3.2), the decay is almost imperceptible, impeded by the compact structure of the foam. Only a few bubbles burst, their size being too small to produce a significant reduction of the column. Approaching the end of the intermediate rest period, the number and size of the exploding bubbles gradually increase, being promoted by the advancing deterioration processes. However, this translates into a lowering of just 4 mm of the foam height. A more drastic collapse of the foam column is observed after the snift valve is opened again: following the modest peak at t' = 4.2, to be attributed exclusively to a swelling of the existing layers, the thickness of the foam reduces of 18 mm within an interval of 11 tenths. The decrease is not continuous but occurs in steps, as it is related to simultaneous ruptures of multiple large bubbles.

The last portion of the curve is characterized by the convergence of the foam thickness to a constant value, i.e. 13 mm. This can be considered as the equilibrium value in the balance between the further deterioration of foam, on the one hand, and the renewed production of bubbles, on the other one, under the conditions achieved with the second decompression step.

4. Conclusions

The foaming phenomena occurring in a carbonated beverage during bottling have been examined with the use of high-speed imaging. It is ascertained that with the adopted decompression sequence, nuclei entrained in the bulk liquid during filling play a major role in the thickening of the foam. Changes occurring in the population of the rising bubbles reflect on the rate of growth of the foam level. In particular, the development of a cloud provided by a global deviation of bubble trajectories determines the achievement of the maximum thickness. Other factors participate in defining the initial growth of the foam, including the conditions at the free surface as decompression initiates, and the onset of foam destabilization processes. Those last phenomena strictly depend on the structure of the foam and influence its subsequent evolution. The end of the process is dominated by the competition between the deterioration of the existing layers and the release of bubbles from sites located on the bottle walls, which allow the establishment of an equilibrium height of the foam.

References

[1] Jones F S, Evans G M and Galvin K P 1999 *Adv. Colloid Interface Sci.* **80** 27–50
[2] Harvey E N, Barnes D K, McElroy W D, Whiteley A H, Pease D C and Cooper K W 1944 *J. Cell. Comp. Physiol.* **24** 1–22
[3] Bińk A K 1993 *Chem. Eng. Sci.* **48** 3585–630
[4] Qu X, Goharzadeh A, Khezzar L and Molki A 2013 *Exp. Therm. Fluid Sci.* **44** 51–61
[5] Ray B, Biswas G and Sharma A 2015 *J. Fluid Mech.* **768** 492–523
[6] Salerno E, Levoni P and Barozzi G S 2015 *J. Phys.: Conf. Ser.* **655** (2015) 012036
[7] Bankoff S G 1958 *AIChE J.* **4** 24–26
[8] Chen P, Wu W and Jones B G 2009 *Nucl. Eng. Des.* **239** 2035–41
[9] Brennen C E 2014 *Cavitation and bubble dynamics* (New York: Cambridge University Press)
[10] Pugh R J 1996 *Adv. Colloid Interface Sci.* **64** 67–142
[11] Malysa K and Lunkenheimer K 2008 *Curr. Opin. Colloid In.* **13** 150–62
[12] Shokribousjein Z, Deckers S M, Gebruers K, Lorgouilloux Y, Baggerman G, Verachtert H, Delcour J A, Etienne P, Rock J, Michiels C and Derdelinckx G 2011 *Cerevisia* **35** 85–101